Electronic Supplementary Information (ESI)

Nanowires-assembled Co_3S_4/Cu_2S@carbon binary metal sulfide hybrid as sodium-ion battery anode displaying high capacity and recoverable rate-performance

Jinyun Liu[a,*], Xiaofei Huang[a], Rui Wang[b,c], Tianli Han[a], Huigang Zhang[b,c]

Experimental

Materials and reagents: Chemicals: $Co(NO_3)_2 \cdot 6H_2O$, urea, ammonium fluoride (NH_4F), ethanol (AR), thioacetamide (TAA), pyrrole, N–methylpyrrolidone (AR, NMP), and $Cu(NO_3)_2 \cdot 3H_2O$ were obtained from Aladdin. All chemicals were used directly without further purification.

Preparation of Co_3S_4/CuS precursors: In a typical experiment, a mixture solution with 0.292 g of $Co(NO_3)_2 \cdot 6H_2O$, 0.18 g of urea, 0.056 g of NH_4F, and 40 mL ethanol was prepared in a 100 mL beaker after magnetically stirring by an agitator for 30 min. Subsequently 0.2412 g of $Cu(NO_3)_2 \cdot 3H_2O$ and 0.3756 g of thioacetamide were added. The obtained solution was transferred to a 50 mL polytetrafluoroethylene reaction autoclave in an oven and heated at 140 ºC for 12 h. After cooling down to room temperature, the sample was washed several times with deionized water/ethanol, and dried at 60 °C for 12 h.

Synthesis of Co_3S_4/CuS @polypyrrole (PPy): 200 mg obtained Co_3S_4/CuS powder and 13 mg SDS were dispersed into 80 mL deionized water, followed by ultrasonic dispersion for 1 h, 40 uL pyrrole monomer sequentially adding to the magnetic stirring for another 1 h. Then 7 mL 0.1 M $(NH_4)_2S_2O_8$ solution were added to the above solution. Keep mixing continuously at room temperature for 4 h to get black deposits. The resultant Co_3S_4/CuS@PPy was collected by centrifugation, washed and dried.

Preparation of Co_3S_4/Cu_2S@NC: The Co_3S_4/CuS@PPy was putted at a quartz boat, and calcined at 400

°C for 8 h with a heat rate of 2.0 °C min^{-1} under Ar/H_2 (95%/5%) atmosphere flow. After calcination, the nanoflower sphere Co_3S_4/Cu_2S@NC were gained. In contrast, the pure Co_3S_4/Cu_2S was produced by the same calcination process using Co_3S_4/CuS as the precursor.

Materials characterization: The phase of the sample was determined by using an X-ray diffractometer (XRD, SMART APEX II Brook, copper target). The morphology was observed by field emission scanning electron microscope (SEM, Hitachi S-8100), and transmission electron microscope (TEM, HT-7700, TecnaiG220S-Twin). A high-resolution TEM (HRTEM) was used to observe the lattice fringes. Energy dispersive X-ray spectroscopy (EDS) was employed for elemental mapping and studying the elemental distribution. X-ray photoelectron spectroscopy (XPS, EscalAB 250) and Raman spectroscopy (Renishaw in Via) were used for characterization. In order to characterize the carbon matrix, Raman spectroscopy (Renishaw in Via) was used. The mass content of carbon was determined by thermogravimetric analysis (TGA, Setaram Labsys Evo SDT Q600). Prior to the BET test, the sample was degassed at 120 °C for 12 h in vacuum to remove water adsorbed on the surface, and then physical adsorption isotherms (adsorption-desorption branch) were recorded using a specific surface area tester (ASAP Micromeritics Tristar 2460).

Electrochemical measurements. The 70 wt% active materials (Co_3S_4/Cu_2S@NC), 20 wt% acetylene black and 10 wt% polyvinylidene fluoride (PVDF) were mixed in a ratio of 7:2:1. The n-methylpyrrolidone (NMP) was used as diluent to disperse the mixture. Evenly-mixed slurry was coated on a Cu foil with a thickness of 9 μm, dried in a vacuum oven at 80 °C for 24 h, and cut into 1.2 mm discs. The counter electrode was sodium, while the diaphragm was fiberglass. The mass loading of the anode was about 1.2 mg cm^{-2}. The coin cells were assembled in an Ar-filled glovebox. Electrolyte contained 1 M $Na_SO_3CF_3$ dissolved in diethylene glycol dimethyl ether. The galvanostatical charge-discharge was tested on Neware Battery system. Cyclic voltammetry (CV, 0.1 mV s^{-1} of sweep rate over the range of 0.2–3 V) and electrochemical impedance spectroscopy (EIS) measurements were performed on an electrochemical workstation (CHI 660E).

For the assembly of full batteries, the $Na_3V_2(PO_4)_3$ (NVP) cathode was prepared by mixing home-made NVP, acetylene black and PVDF with a weight ratio of 8:1:1 in NMP to form a slurry, which was cast onto aluminum foil. The electrolyte was 1 M sodium hexafluorophosphate ($NaPF_6$) in diethylene

glycol dimethyl ether.

First-principle calculations: Vienna Ab initio Simulation Package (VASP) was employed for the first-principle calculations. Structure optimization was accomplished by the Perdew-Burke-Ernzarhof exchange–correlation function under generalized gradient approximation and project-augmented wave atom potentials, where the Coulomb U and exchange J parameters were considered ($U_{eff} = U - J$). To simulate the Co_3S_4/Cu_2S hybrid composite, a vacuum layer around 15 Å in the *z* direction was inserted to avoid the periodic effect. The primitive structures of CoS and Cu_2S were obtained from Material Project. During the optimization process, the cutoff energy of the plane-wave basis was set as 500 eV, and the structural optimization process stopped when an energy convergence was lower than 10^{-5} eV and the atomic force was less than 0.01 eV/Å. Brillouin zone integration was performed using a 3 × 3 × 1 *k*-point mesh.

Equations:

Intercalation (discharge):

$Cu_2S + xNa^+ + xe^- \rightarrow Na_xCu_2S$ (1)

$Co_3S_4 + xNa^+ + xe^- \rightarrow Na_xCo_3S_4$ (2)

$Na_xCu_2S + (2 - x)Na^+ + (2 - x)e^- \rightleftharpoons 2Cu + Na_2S$ (3)

$Na_xCo_3S_4 + (8 - x)Na^+ + (8 - x)e^- \rightleftharpoons 4Na_2S + 3Co$ (4)

Deintercalation (charge):

$Na_xCu_2S \rightarrow Cu_2S + xNa^+ + xe^-$ (5)

$Na_xCo_3S_4 \rightarrow Co_3S_4 + xNa^+ + xe^-$ (6)

$$D_{na^+} = \frac{4}{\tau\pi}\left(\frac{n_m V_m}{S}\right)^2 \left(\frac{\partial E_S}{\partial E_\tau}\right)^2 \quad (7)$$

where τ represents current pulse time (h), V_m shows molar volume of active material, S is electrode area, ΔE_S indicates potential change between discharge pulse and open circuit state, and ΔE_τ stands for voltage change.

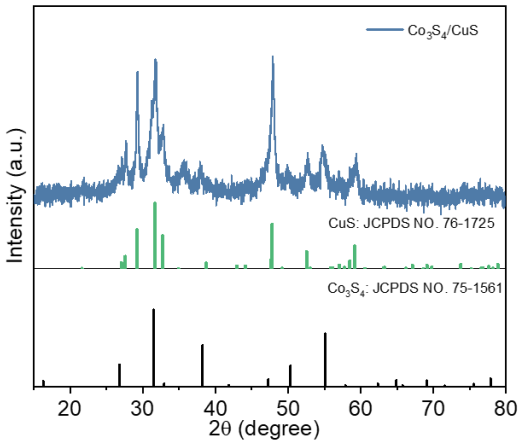

Fig. S1 XRD patterns of Co_3S_4/CuS.

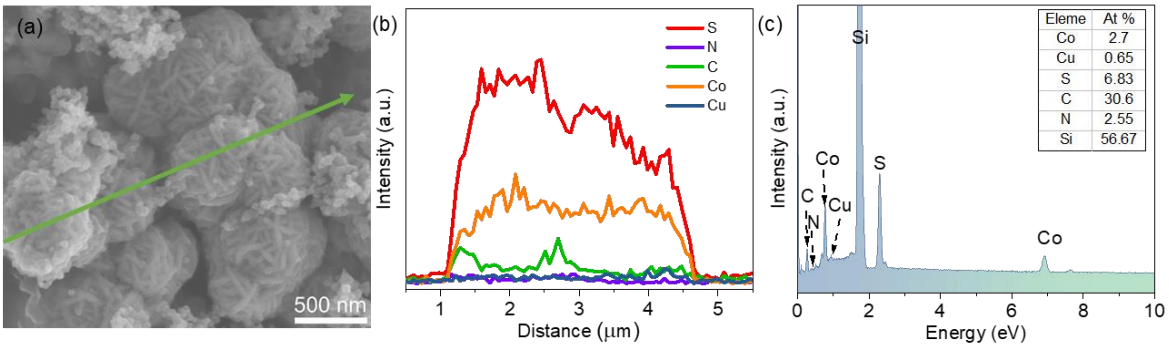

Fig. S2 (a) SEM image, (b) line-scanning curves, and (c) EDS spectrum of Co_3S_4/Cu_2S@NC.

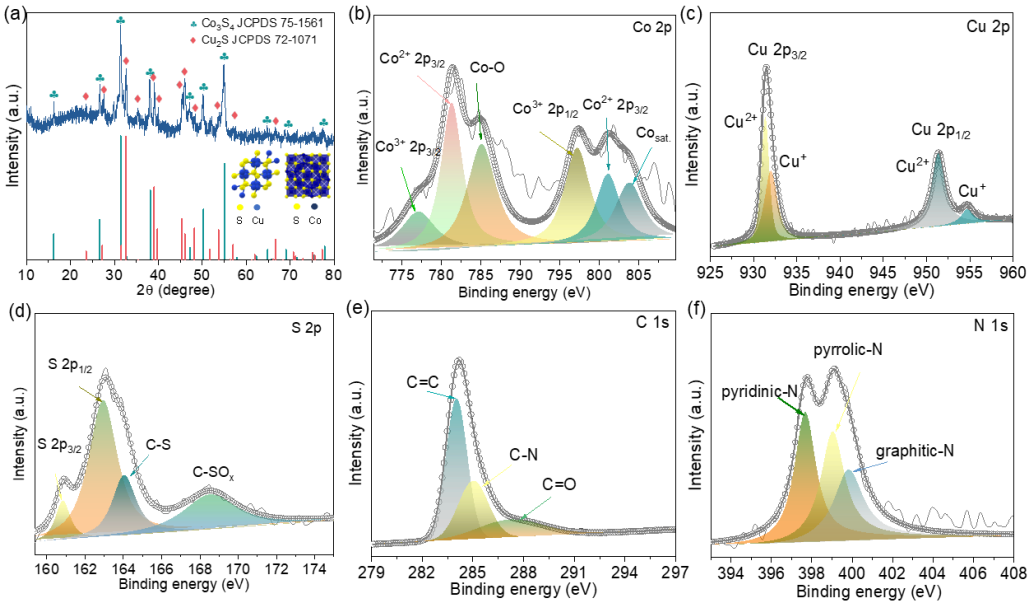

Fig. S3 (a) XRD patterns, XPS spectra of (b) Co 2p, (c) Cu 2p, (d) S 2p, (e) C 1s, (f) N 1s.

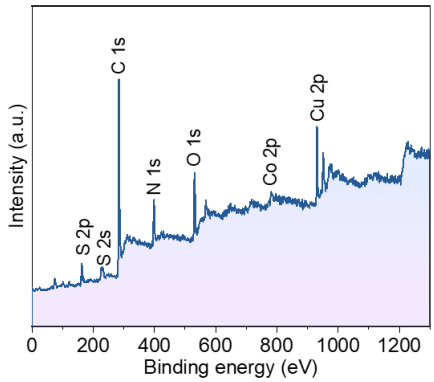

Fig. S4 XPS survey spectrum of Co_3S_4/Cu_2S@NC.

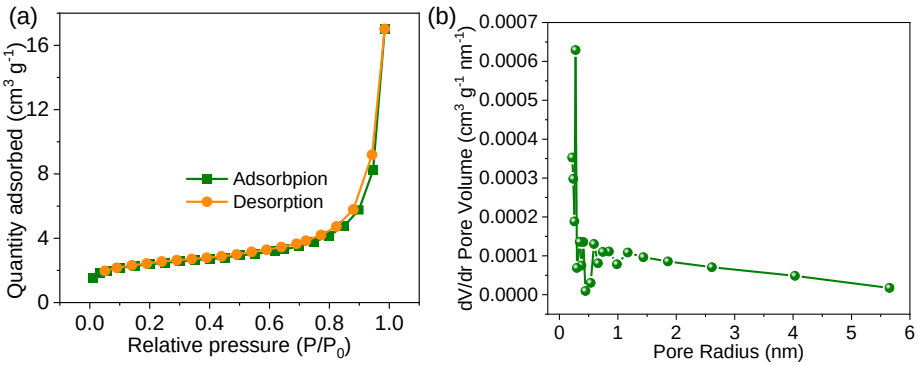

Fig. S5 (a) The N_2 adsorption-desorption isotherms of the composite. (b) The pore-size distribution.

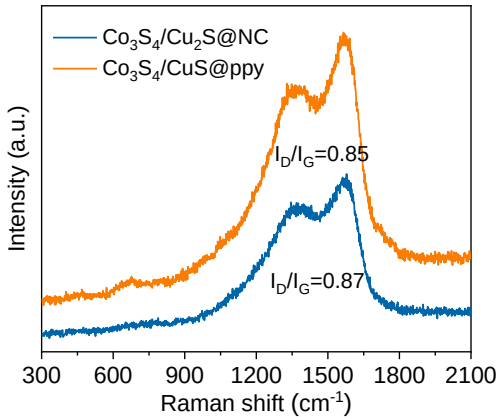

Fig. S6 Raman spectrum of Co_3S_4/Cu_2S@NC and Co_3S_4/CuS@PPy.

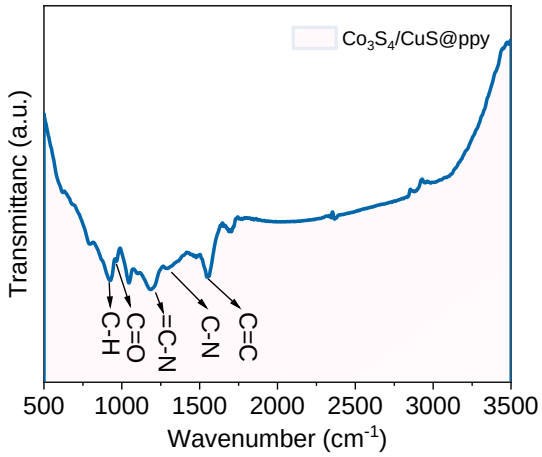

Fig. S7 FTIR spectra of Co_3S_4/CuS@PPy hybrid.

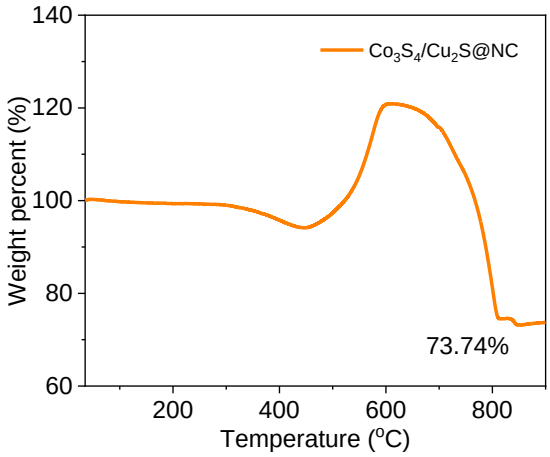

Fig. S8 TGA curve of Co_3S_4/Cu_2S@NC.

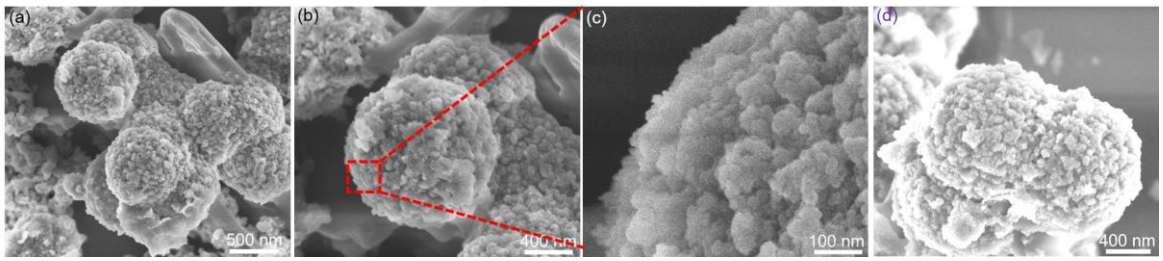

Fig. S9 SEM images of the Co_3S_4/Cu_2S@NC after cycling (a-c) 200 times and (d) 350 times at 1 A g^{-1}.

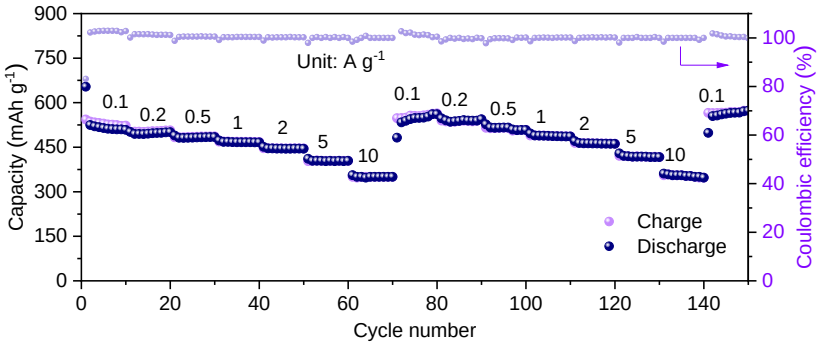

Fig. S10 Rate-performance of Co_3S_4/Cu_2S@NC at 0.1-10 A g^{-1}.

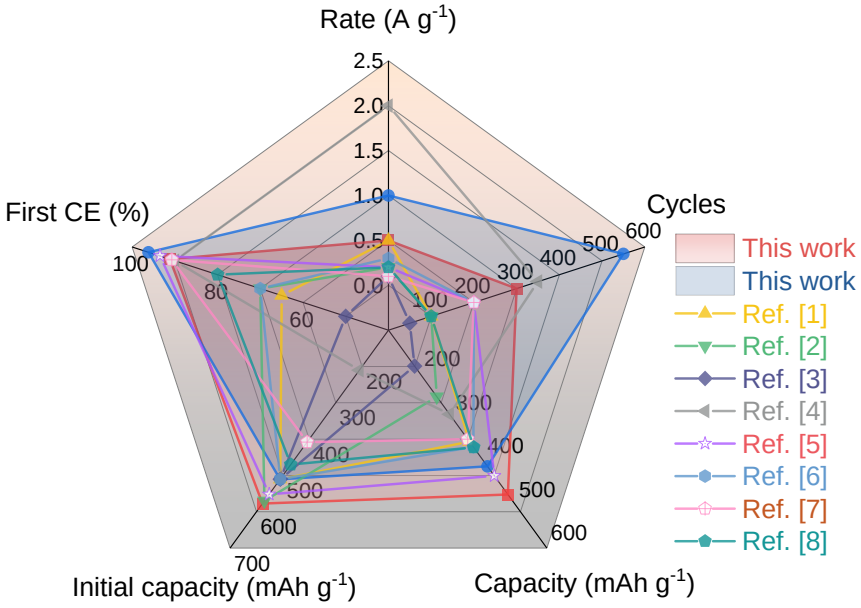

Fig. S11 Radar graph of some reported anodes for Na-ion batteries.

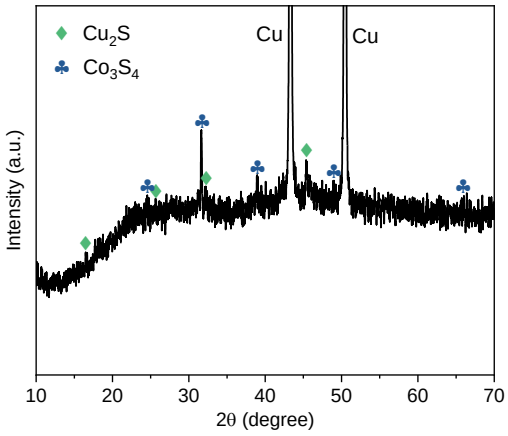

Fig. S12 XRD pattern of Co_3S_4/Cu_2S@NC after cycling.

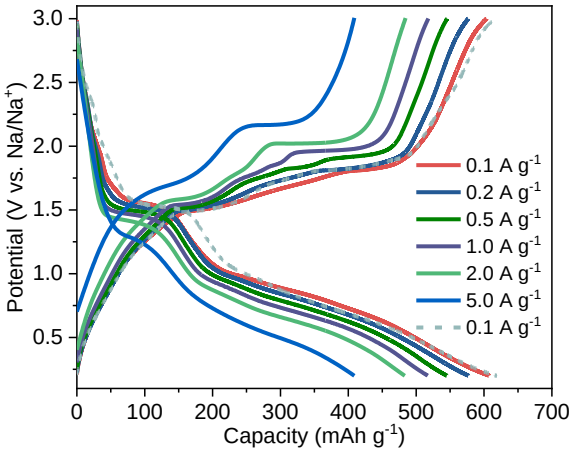

Fig. S13 Galvanostatic discharge-charge curves of Co_3S_4/Cu_2S@NC at different current densities (0.1–5 A g^{-1}).

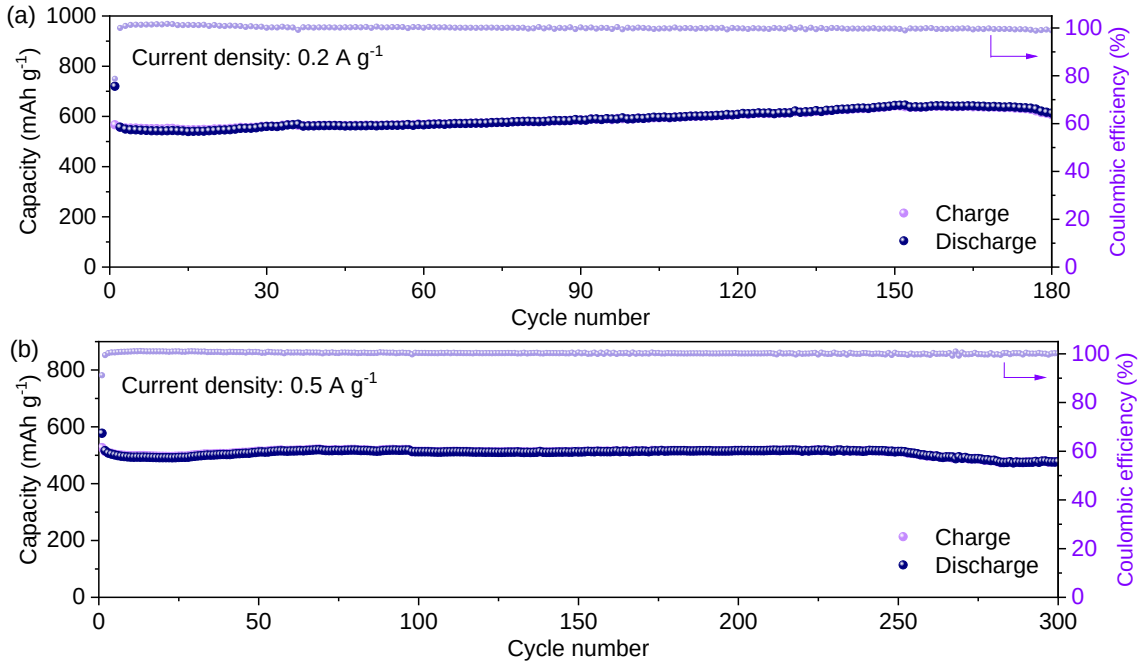

Fig. S14 Cycling performance of Co_3S_4/Cu_2S@NC anode at (a) 0.2 and (b) 0.5 A g^{-1}.

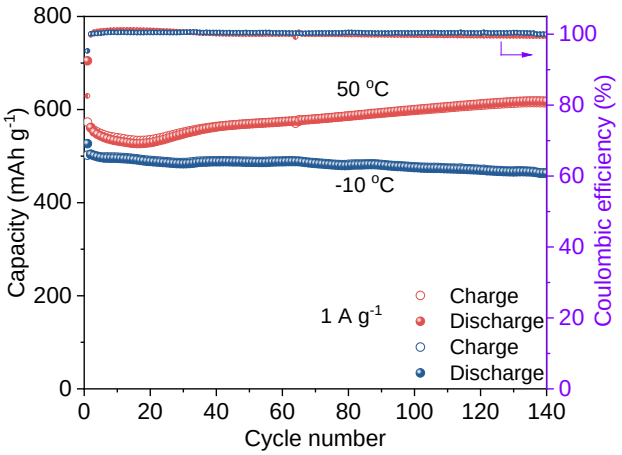

Fig. S15 Cycling performance of the battery with the Co_3S_4/Cu_2S@NC as anode under (b) 50 °C and (c) –10 °C at 1.0 A g^{-1}.

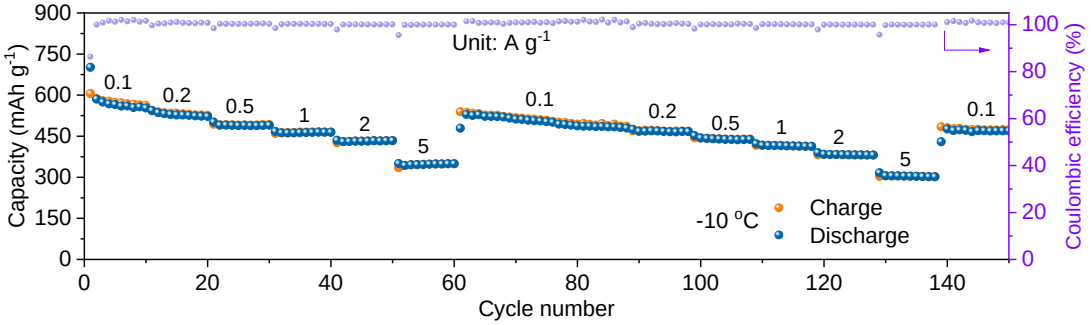

Fig.S16 Rate-performance of the Co_3S_4/Cu_2S@NC under –10 °C.

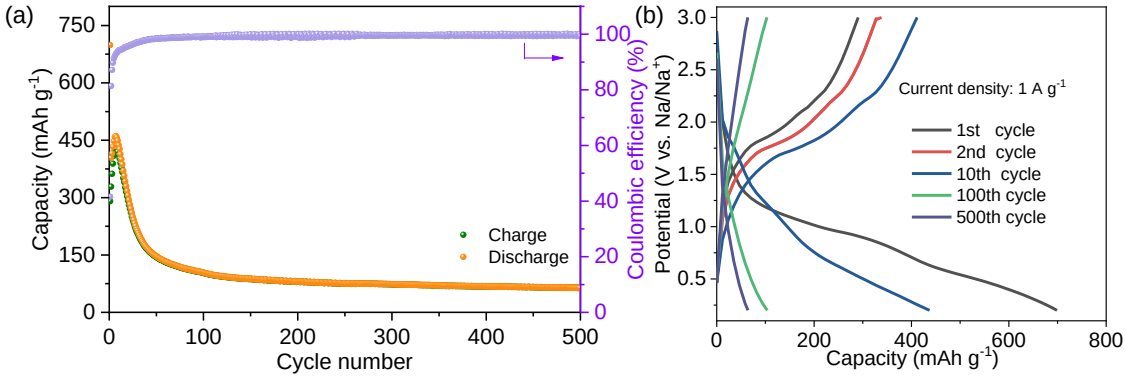

Fig. S17 (a) Cycling performance and (b) GCD curves of the Co_3S_4/Cu_2S@NC at 1 A g^{-1} in the carbonate electrolyte (1 M $NaClO_4$ in EC:DEC(1:1)vol+ 5% FEC).

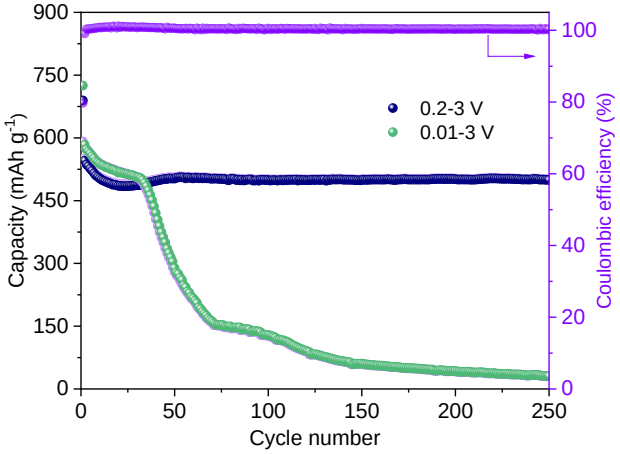

Fig. S18 Cycling performance of Co_3S_4/Cu_2S@NC under different voltage windows at 1.0 A g^{-1}.

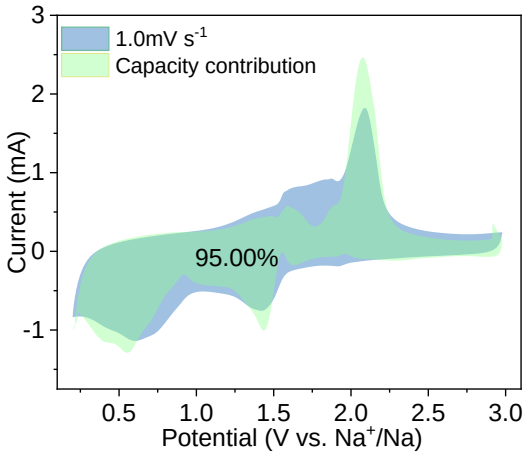

Fig. S19 CV curve with the pseudocapacitive contribution at 1.0 mV s^{-1}.

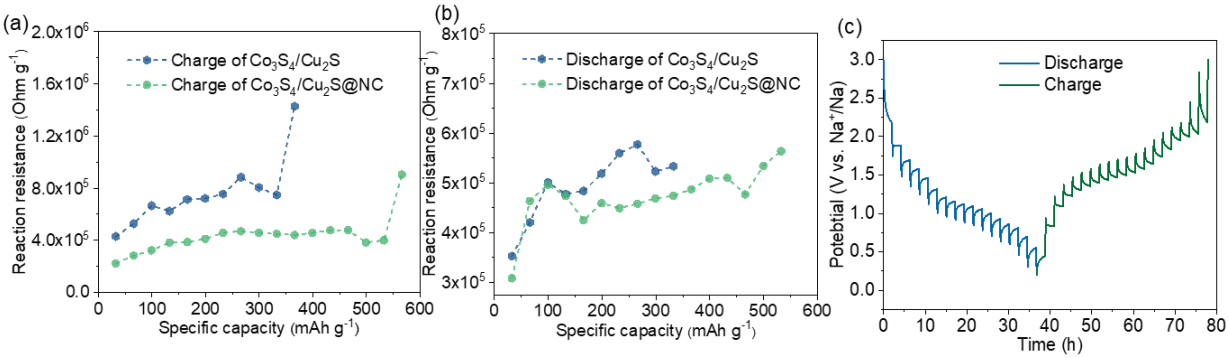

Fig. S20 *In situ* reaction impedances of Co_3S_4/Cu_2S@NC and Co_3S_4/Cu_2S during (a) charge and (b) discharge. (c) GITT time–potential distributions of Co_3S_4/Cu_2S@NC.

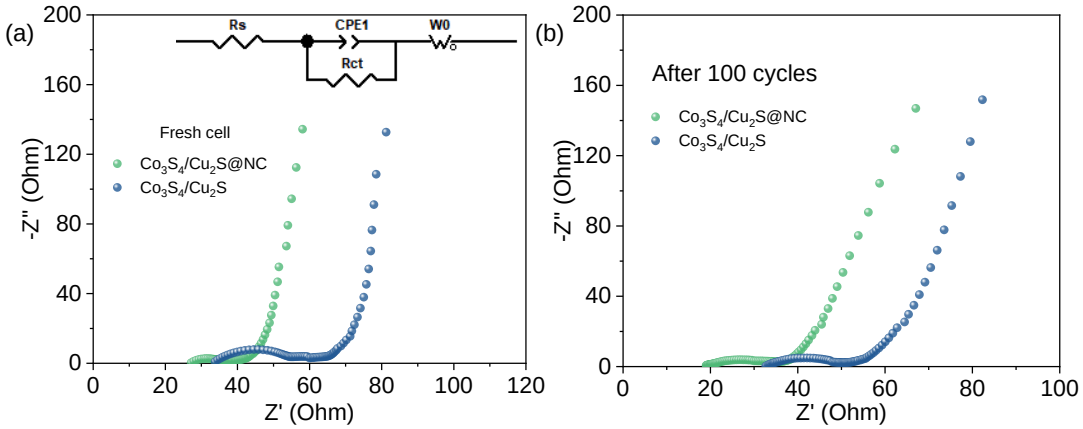

Fig. S21 EIS spectra of the Co_3S_4/Cu_2S@NC and Co_3S_4/Cu_2S (a) before and (b) after 100 cycles at 1 A g^{-1}. The inserts display the equivalent circuits.

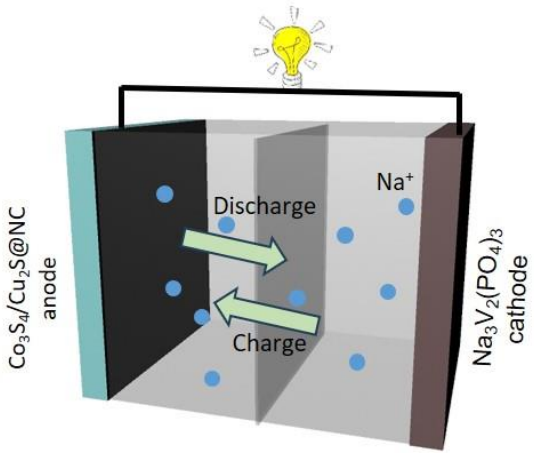

Fig. S22 Schematic diagram of of full cell assembled by Co_3S_4/Cu_2S@NC anode and NVP cathode.

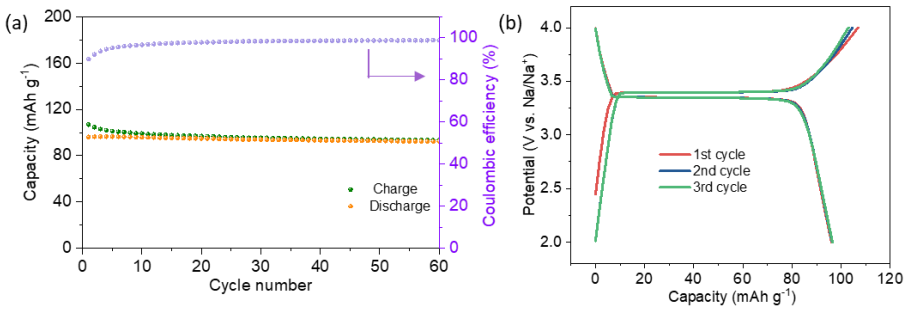

Fig. S23 The electrochemical properties of the $Na_3V_2(PO_4)_3$.

Table S1. Comparison on the electrochemical performance of some Na-ion battery anodes.

Anode materials	Current density ($A\ g^{-1}$)	Capacity ($mAh\ g^{-1}$)	Cycle number	Ref.
Co_3S_4/Cu_2S@NC	0.5	477.1	300	This work
	1.0	412.3	550	
Co_3S_4/CNTs	0.5	355.9	100	[1]
Co_3S_4@polyaniline	0.2	252.5	100	[2]
Cu_2S@N,S dual-doped carbon matrix	0.1	182.3	50	[3]
Cu_2S/CNT	2.0	293	350	[4]
Cu_2S@ZnS/C	0.2	434	200	[5]
Cu_2S@carbon@MoS_2	0.3	368	200	[6]
Cu_2S twin-daffodil	0.1	350	200	[7]
Cu_2S hollow spheres	0.2	369	100	[8]

Reference

1 D. N. Liu, A. P Hu, Y. F. Zhu, S. P. Zhou, Y. Duan, Q. L. Tang, W. N. Deng, X. H. Chen, *Ceram. Int.* 2019, **45**, 3591-3599.

2 Q. Zhou, L. Liu, Z. F. Huang, L. G. Yi, X. Y. Wang, G. Z. Cao, *J. Mater. Chem. A* 2016, **4**, 5505-5516.

3 Q. W. Chen, M. M. Ren, H. Xu, W. L. Liu, J. P. Hei, L. W. Su, L. Z. Wang, *ChemElectroChem.* 2018, **5**, 2135-2141.

4 J. Ren, G. Q. Ling, H. Guo, F. Zhang, W. H. Tian, P. Bai, J. Q. Han, R. P. Ren, Y. K. Lv, *J. Alloys Compd.* 2023, **953**, 170161.

5 B. A. Yu, Y. X. Ji, X. Hu, Y. J. Liu, J. Yuan, S. Lei, G. B. Zhong, Z. X. Weng, H. B Zhan, Z. H. Wen, *Chem. Eng. J.* 2022, **430**, 132993.

6 Y. J. Fang, D. Y. Luan, Y. Chen, S. Y. Gao, *Angew Chem. Int. Ed.* 2020, **59**, 7178–7183.

7 T. Li, H. Wu, H. Li, S. H. Chen, D. H. Zhang, F. Xu, *Mater. Chem. Phys.* 2020, **248**, 122934.

8 J. B. Wang, J. Okabe, K. Urita, ;I. Moriguchi, M. D. Wei, *J. Electroanal. Chem.* 2020, **874**, 114523.